The Third Generation (G3) Dual-Modal and Dual Sensing Mechanisms (DMDSM) Pretouch Sensor for Robotic Grasping*

Cheng Fang, Shuangliang Li, Di Wang, Fengzhi Guo, Dezhen Song, and Jun Zou

***Abstract*—Fingertip-mounted pretouch sensors are very useful for robotic grasping. In this paper, we report a new (G3) dual-modal and dual sensing mechanisms (DMDSM) pretouch sensor for near-distance ranging and material sensing, which is based on pulse-echo ultrasound (US) and optoacoustics (OA). Different from previously reported versions, the G3 sensor utilizes a self-focused US/OA transceiver, thereby eliminating the need of a bulky parabolic reflective mirror for focusing the ultrasound and laser beams. The self-focused laser and ultrasound beams can be easily steered by a (flat) scanning mirror which expands from single-point ranging and detection to areal mapping or imaging. To verify the new design, a prototype G3 DMDSM sensor with a scanning mirror is fabricated. The US and OA ranging performances are tested in experiments. Together with the scanning mirror, thin wire targets made of same or different materials at different positions are scanned and imaged. The ranging and imaging results show that the G3 DMDSM sensor can provide new and better pretouch mapping and imaging capabilities for robotic grasping than its predecessors.**

I. Introduction and Related Work

Robust and reliable grasping of unknown objects is a grand challenge in the field of robotics [1] [2]. When robots expand application domain from industry floor to a wide range of domestic work, the prior knowledge of objects is often not available, making sensor-less grasping difficult [3] [4]. Sensor-based grasping approaches rely on sensors to quickly provide information about object relative pose and material/structure. Ideally, assisted by the pretouch sensors, robotic fingers ought to dynamically adjust the grasping plan corresponding to subtle changes in object pose right before grasping. Moreover, sensors should quickly provide the information about material-type and interior structure, which helps better anticipate the force distribution, impact characteristics, and friction coefficients for a more robust grasping plan. Unfortunately, to a large degree, current sensors cannot meet these requirements. Cameras and laser range finders suffer from the occlusion caused by closing-in robotic grippers themselves [5] or having a near-range blind zone [6] [7] [8] [9]. Tactile [10] [11] and force sensors [12] require gripper finger physically contacting with objects, which may change object poses, damage its surface, and thus lead to grasping failure. Therefore, contactless pretouch sensing is more desirable. Recent development of proximity sensors based on optical, electric-field, and ultrasound signals have made great progress in this direction, but they still suffer from sensing modalities and/or limited types of target materials. For example, electric-field sensors are challenged by targets with dielectric constants close to that of air [13] [14] [15] [16]. Optical sensors lack lateral resolution and cannot handle optically-transparent or highly-reflective targets [17] [18] [19] [20]. Ultrasound-based sensors fail on sound absorbing or reflective materials [21] [22] [23] [24].

Previously, we demonstrated a dual-modal and dual sensing mechanisms (DMDSM) pretouch sensor design for near-distance ranging and material sensing based on pulse-echo ultrasound (US) and optoacoustics (OA) [25] [26] [27] [28] [29]. In both modalities, the temporal delays of US/OA signals allow the determination of the target-sensor distance for ranging, while their frequency spectra provide distinctive features for classifying the target material/structure. To improve the lateral resolution, the planar laser and ultrasound beams generated by the flat US/OA transceiver are reflected and focused with a right-angle parabolic mirror (Fig. 1(a)). While this design provides a simple and effective solution for single-point detection, the bulky parabolic mirror cannot steer laser and ultrasound beams over the target surface, which otherwise would be very useful for fast mapping or imaging the detailed features for facilitating the grasping.

To address this issue, we report a new (G3) DMDSM sensor, where the US/OA transceiver is updated from the previous flat design to a focused one (Fig. 1(b)) to allow us to remove the bulky parabolic mirror. When combining with a 2D scanning mirror, the G3 DMDSM sensor expands from the limited single-point ranging and sensing to new areal mapping and imaging capabilities. In this work, a prototype G3 DMDSM sensor is designed and fabricated. Its ranging performances are characterized and compared with those of the previous versions. Thin wire targets made of same or different materials at different locations are successfully scanned and imaged. The experimental results show that the G3 DMDSM sensor can provide new pretouch mapping and imaging capabilities to enhance robotic grasping.

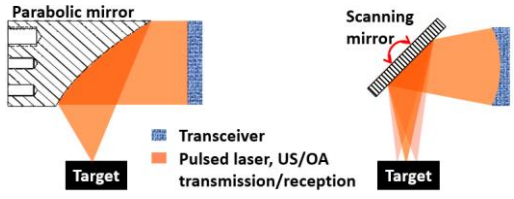

Figure 1. Digrams showing the different designs of (a) G2 and (b) G3 DMDSM sensors.

*The research is supported in part by National Science Foundation under NRI-1925037.

C. Fang, S. Li, and J. Zou are with the Electrical and Computer Engineering Department, Texas A&M University, College Station, TX 77843, USA (e-mails: {fangchengok2007, slli940922, junzou}@tamu.edu).

D. Wang, F. Guo, and D. Song are with the Computer Science and Engineering Department, Texas A&M University, College Station, TX 77843, USA (e-mails: ivanwang@tamu.edu, fengzh_g@tamu.edu, dzsong@cs.tamu.edu).

II. Sensor Development

A. Sensor Design

Figure 2 illustrates the schematic design of the G3 DMDSM sensor. It consists of a focused US/OA transceiver in a co-centered and co-axial configuration. For US ranging and sensing, the (green) pulsed laser beam from the light source is expanded by two lenses to illuminate the spherically-shaped black tape layer. Upon its absorption, the pulsed laser beam generates a heat pulse and subsequent thermal expansion and contraction in the black tape layer, which transmit a focused (by the spherical shape) ultrasound pulse to the target (after being reflected by the flat scanning mirror). The echo signals travelling back along the reverse path are collected by the ring transducer with a focusing acoustic lens attached in front. For OA ranging and sensing, the inner part of the pulsed laser beam is focused by a small lens and passes through the center hole of the black tape layer onto the target (after being reflected by the flat scanning mirror). The excited optoacoustic signal travels along the reverse path and is collected by the same ring transducer. One laser pulse triggers the collection of both US and OA signals without mixing with each other [25]. This is because the US signals arrive at the transducer after a round trip, while the OA signal only goes through a single trip, which results in a large difference in their time delays. With a 2D scanning mirror, the focused laser and US/OA beams can be reflected and scanned over the target with customized patterns. It is worth mentioning that the mirror-transceiver distance (d_1) can be adjusted to enable the ranging even when the sensor package (as the gray dashed line in Fig. 2) contacts the target.

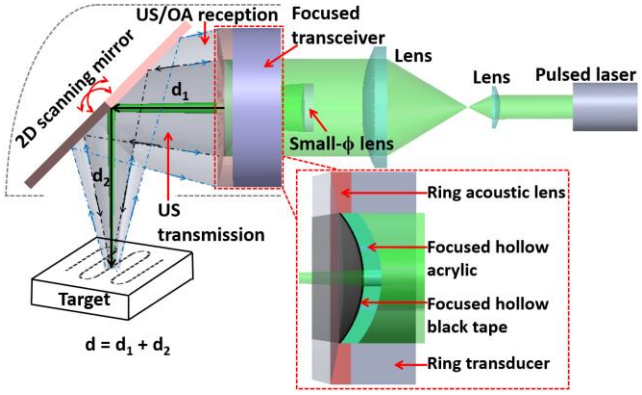

Figure 2. Schematic design of the G3 DMDSM sensor with a zoom-in cross-section view of the redesigned focused US/OA transceiver. d_1 and d_2 is the distance from the mirror reflection center point to the transceiver and the scanning point on target, respectively.

B. Sensor Construction

Fig. 3 shows the fabricated prototype of the G3 DMDSM sensor (weight ≈ 13.7 grams), which consists of a 3D-printed housing (length ~ 27 mm, ϕ ~ 26 mm), a small-ϕ glass lens (Fig. 3(c)), and a focused US/OA transceiver. The focused US transmitter consists of a molded optically-transparent acrylic plate (1.6-mm thick) as the supporting substrate and a black vinyl electrical tape (0.1-mm thick) as the laser-absorption layer (Figs. 3(b) and 3(c)). Both acrylic and vinyl have low Young's modulus (several GPa) and high internal damping, which allows effective generation of wideband low-MHz ultrasound signals. The acrylic plate and black vinyl tape are molded by one pair of matched plano-convex and concave glass lenses with a diameter of 12 mm and spherical radius of 9.42 mm, which provides an acoustic numerical aperture (NA) around 0.64. A center hole with a 1.5-mm diameter is drilled on the acrylic plate and black vinyl tape to allow the pulsed laser to pass through, which is focused by the small-ϕ (6-mm) glass lens in advance (Fig. 2) . To better collect the US echoes and OA signals from the target, a ring-shaped epoxy acoustic lens (with a focal length around 4 cm) is added to the front of the flat ring-PZT (lead zirconate titanate) transducer (with a 19.6-mm outer diameter and 12-mm inner diameter). The epoxy lens also serves as the acoustic impedance matching layer to improve the acoustic coupling efficiency between air and PZT. In addition, soft PZT composite is used to fabricate the ring transducer, which provides a higher electromechanical coupling factor and wider acoustic bandwidth than the hard PZT previously used in the G2 sensor.

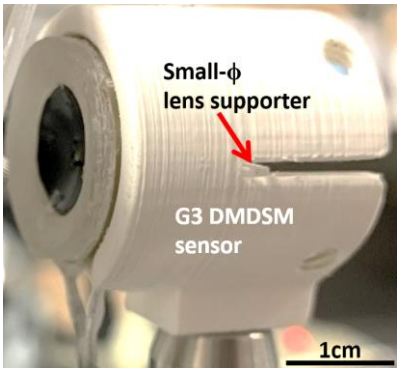

(a)

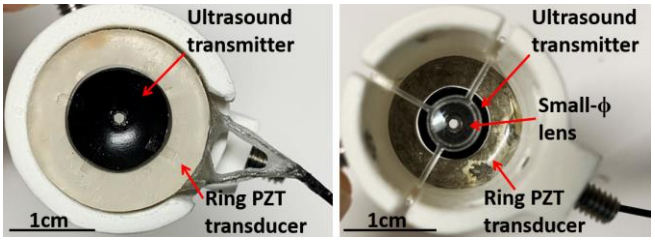

(b) (c)

Figure 3. Photographs of the (a) side, (b) front, and (c) back view of the fabricated prototype of the G3 DMDSM sensor. The focused ultrasound transmitter is housed inside the inner hole of the ring PZT transducer.

C. Sensor Test and Characterization

Fig. 4(a) shows the setup for characterizing the US/OA performances of the G3 DMDSM sensor. A Q-switched 532nm Nd:YAG pulsed laser is used as the light source. It has a pulse repetition rate (PRR) of 10 Hz, a pulse duration of 8 ns, and an average pulse energy around 2.5 mJ/pulse. One laser pulse initiates simultaneous US and OA data acquisition. The US and OA signals are received by the focused ring transducer, amplified by a preamplifier, and then recorded by an oscilloscope. A photo detector is used to detect the laser pulse and generate a trigger signal to synchronize the data acquisition. Fig. 4(b) shows a representative US/OA signal from an aluminum block as the target. The time delays of the 1st OA signal, the US signal, and the 2nd OA signal (the reflection of the 1st OA signal after a round trip) are around 75 µs, 156 µs, and 221 µs, respectively.

To characterize the reception bandwidth of the focused ring transducer, a 0.4-mm pencil lead is used as the target. The distance (d) between the US/OA transceiver and pencil lead is around 3 cm. Upon illumination of focused laser pulses, the pencil lead generates short-pulse OA signals with a wide bandwidth. A representative OA waveform and its frequency spectrum received by the transducer are shown in Figs. 4(c) and 4(d), respectively, which indicates a wide bandwidth consisting of four frequency bands centered around four resonance frequencies of 52 kHz, 412 kHz, 748 kHz, and 1164 kHz. Next, the collective acoustic bandwidth of the US transceiver is characterized, which is determined by both the transmission from the black tape and also the reception of the transducer. A piece of flat 1-mm-thick glass slide serves as the target. Because it has very low optical absorption, the generation of OA signals is minimized. The distance (d) between the US/OA transceiver and glass slide is around 3 cm. A representative US waveform and its frequency spectrum received by the transducer are shown in Figs. 4(e) and 4(f), respectively, which indicates a narrower collective bandwidth consisting of three frequency bands centered around three resonance frequencies around 56 kHz, 272 kHz, and 428 kHz, which is due to the lower-frequency response of the US transmitter consisting of the molded acrylic plate and black tape.

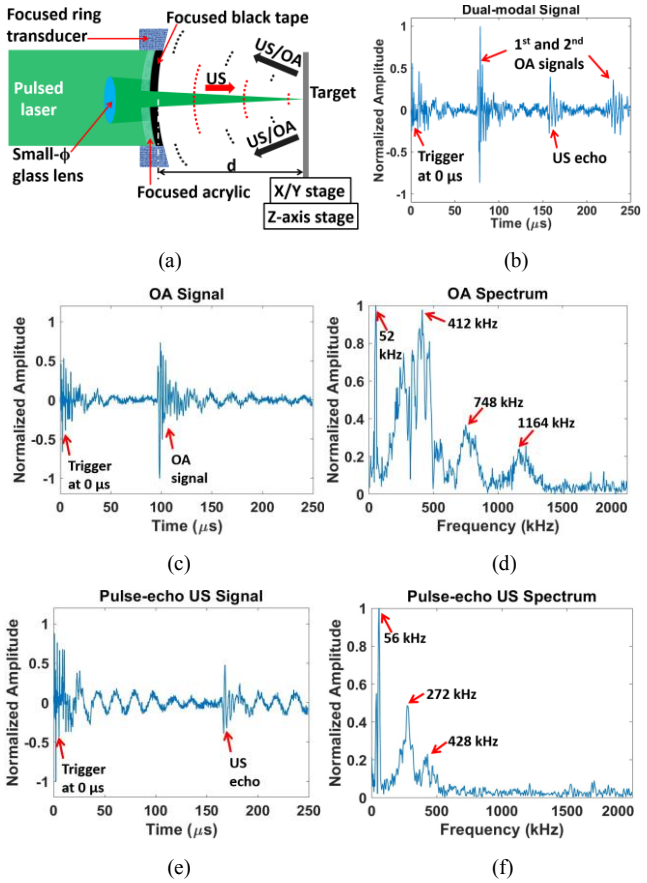

Figure 4. (a) Diagram of the setup to characterize the G3 DMDSM sensor. (b) Representative waveform of the received US and OA signals from an aluminum block through air. Representative (c) OA waveform and (d) frequency spectrum from a 0.4-mm-ϕ pencil lead. Representative (e) US waveform and (f) frequency spectrum from a 1-mm-thick flat glass slide.

III. Ranging Experiment and Results

A. *Pulse-echo Ultrasound Ranging*

The same testing setup (Fig. 4(a)) is used to characterize the US and OA ranging performances of the G3 DMDSM sensor. For US ranging, a piece of 1-mm-thick flat glass slide is used as the target. The distance (d) between the US/OA transceiver and the glass slide is increased from 4.0 mm to 80.0 mm (the maximum distance range of the X/Y stage) with an increment of 2.0 mm. The measured (delay-calculated) distance vs. the actual distance (d) and their deviations are shown in Figs. 5(a) and 5(b), respectively. With a second-order polynomial fitting and calibration, the deviation is less than 0.24 mm where d increases from 4.0 mm to 78.0 mm. The ultrasound echo signal becomes undetectable at $d <$ 4.0 mm, due to the limited reception angle of the focused ring transducer. Without the X/Y stage, the maximal ranging distance of pulse-echo ultrasound modality is roughly measured as ~156 mm (Fig. 5(c)). The same setup is used to quantify the lateral resolution of the US ranging, except that the glass slide target is replaced by an optically-transparent optical fiber with a diameter of 1.0 mm. After repeating the lateral scans at different distance (d) from 26.0 mm to 36.0 mm, the ultrasound lateral resolution is determined by the minimal acoustic focal diameter (Fig. 5(d)), indicating the lateral resolution around 1.04 mm at the focal length d = 31.0 mm. The measured focal zone is around 10.0 mm where d is from 26.0 mm to 36.0 mm, with maximum ranging deviation around 0.1 mm.

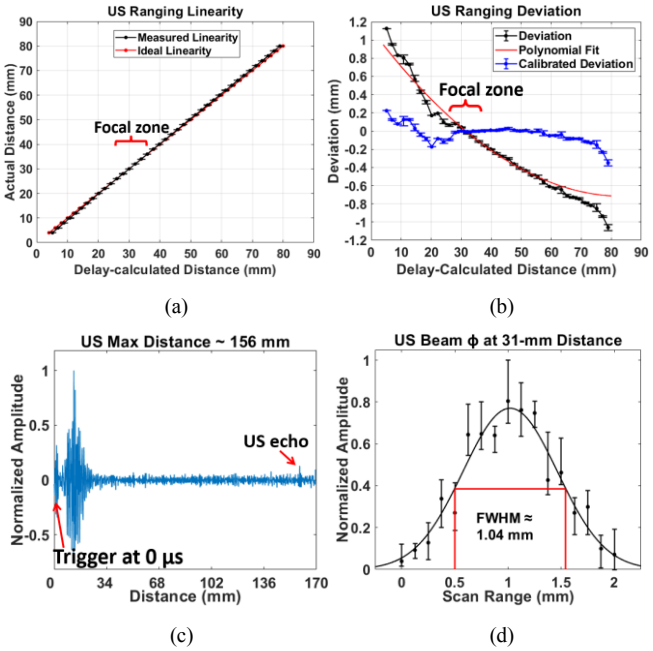

Figure 5. (a) Comparison between measured (in black) and actual (in red) distances. (b) Deviation of the measured distance from the actual distance. (c) Maximal pulse-echo ultrasound ranging distance ~ 156 mm. (d) US lateral resolution of 1.04 mm determined by the minimal acoustic focal diameter at d = 31 mm.

B. *Optoacoustic Ranging*

The OA ranging performance of the G3 sensor is characterized by using a black-paint-coated box as the target (Fig. 4(a)). The distance (d) between the US/OA transceiver and the box is increased from 10.0 mm to 80.0 mm with an

increment of 2.0 mm. The measured distance vs. real distance (d) and their deviations are shown in Figs. 6(a) and 6(b), respectively. With the polynomial fitting and calibration, the deviation is less than 0.2 mm where d is from 10.0 mm to 80.0 mm. OA signal becomes undetectable at distance < 10.0 mm, due to the limited reception angle of the focused ring transducer. After removing the X/Y stage, the maximal OA ranging distance is roughly measured as ~161 mm (Fig. 6(c)). The same setup is used to quantify the optoacoustic lateral resolution, except that the black box is replaced by a 0.4-mm-ϕ pencil lead. The pencil lead is laterally scanned at different distance (d) from 16.0 mm to 80.0 mm. The optoacoustic lateral resolution is determined by the minimal laser focal diameter (Fig. 6(d)), indicating a lateral resolution ~0.29 mm at the focal length (d = 51.0 mm). The lateral resolution of OA is much better than that of US (~1.04 mm), mainly because of a much smaller laser focal spot. The measured OA focal zone is around 50.0 mm where d is from 26.0 mm to 76.0 mm, with ranging deviation less than 0.13 mm. The focal zone of OA is much larger than that of US (~10 mm), mainly because of the smaller laser NA than US. Nevertheless, the two focal zones are overlapped at distance (d) from 26.0 mm to 36.0 mm, providing a 10-mm shared working range with optimal lateral resolutions of both modalities.

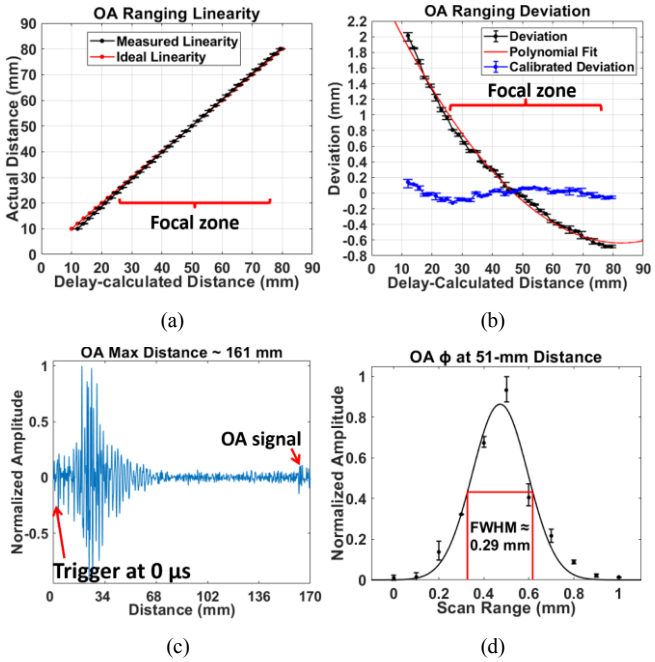

Figure 6. (a) Comparison between the measured (in black) and the real (in red) distances. (b) Deviation of the measured distance from the real distance. (c) Maximal OA ranging distance ~ 161 mm. (d) OA lateral resolution of 0.29 μm determined by the minimal OA focal diameter at d = 51.0 mm.

Table 1 lists the ranging performances of the G1, G2, G3 DMDSM sensors, with improvements marked in green. For both US and OA ranging of G3 sensor, the lateral resolution is deteriorated, but the focal zone and working distance are greatly enlarged, which provide a much larger overlapped range of US and OA modalities. This is because of the smaller NA of the focused transceiver than that of the parabolic mirror. Also, with the assistance of curve fitting and calibration, the ranging deviation of the G3 sensor is greatly reduced.

TABLE I. THE RANGING PERFORMANCES COMPARISION OF THE G1, G2 AND G3 DMDSM SENSORS

Ranging Performances	G1 Sensor [27]	G2 Sensor [25]	G3 Sensor
US Focal Zone (mm)	2.0	3.0	**10**
US Max Deviation within Focal Zone (mm)	0.24	0.29	**0.1**
US Lateral Resolution (mm)	1.04	0.60	1.04
US Working Distance (mm)	0-6.5	0.5-11	**4-156**
OA Focal Zone (mm)	1.0	1.0	**50**
OA Max Deviation within Focal Zone (mm)	0.12	0.20	**0.13**
OA Lateral Resolution (μm)	95.0	61.7	290
OA Working Distance (mm)	5-8	5-7	**10-161**
Overlap of US/OA focal zone (mm)	0	1.0	**10**

IV. IMAGING EXPERIMENTS

A. 2D Scanning Mirror

To demonstrate the scanning and imaging with the G3 sensor, a two-axis flat scanning mirror is designed and fabricated to enable the steering of the co-centered and co-axial dual-modal beams. The scanning mirror consists of a reflective mirror plate mounted on a fixed-frame with four side torsion hinges and actuated by inductor coils to enable fully operation without any mechanical joints [30]. A piece of 20 mm × 20 mm double-side-polished silicon wafer with 200-μm thickness is used as the mirror plate for optical and acoustic reflection. Limited by the low 10-Hz PRR of the pulse laser, the scanning mirror is driven by two DC bias voltages under the quasistatic condition. The DC bias is applied to the inductor coils to steer the mirror plate step-by-step along the two axes. In the imaging experiments, the two axes are tilted by around ±16º under ±3 V DC bias, and ±4º under 0 - 2 V DC bias, respectively. The voltage step is 0.2 V for both axes, and the imaging area is around 8 mm (pan) × 2 mm (tilt).

B. 2D Imaging of Different Thin Targets

An optically-transparent optical fiber, a black coaxial cable, and a black cotton wire placed at similar height are used as targets (Fig. 7(a)). Their diameters are all around 1 mm, and the lateral spacing is 2 mm, making the air gap between two adjacent targets around 1 mm (Fig. 7(a)). For each data, the US/OA signals are averaged by 128/16 times, respectively to improve the signal-to-noise ratio (SNR). The 2D US and OA images (Figs. 7(b) and 7(c)) are reconstructed based on the normalized signal amplitude at each location (pixel), which is indicated by the color bar. In the US image, the optical fiber appears wider than the black coaxial cable, and the soft cotton wire is hardly detected. This is because of their different acoustic impedance and thus different acoustic reflectivity (optical fiber > cable plastic jacket >> cotton wire). In the OA image, the black coaxial cable and black cotton wire are resolved clearly, and the transparent optical fiber could not be detected, due to their different optical absorptivity (cable plastic jacket ≈ cotton wire >> optical fiber). There exist some variations in the signal strength across the image, which would be due to the slight height variations caused by different topographic features of the targets.

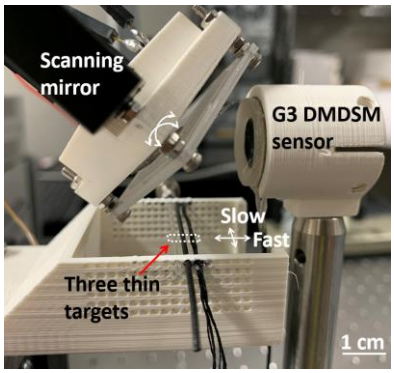

(a)

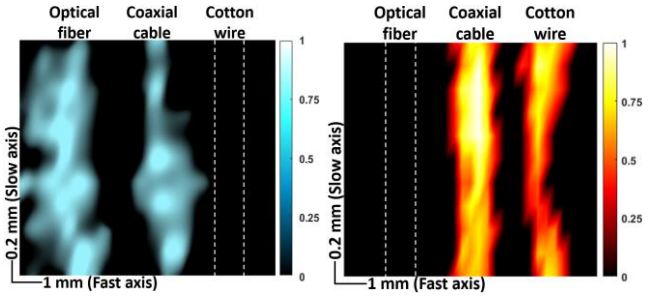

(b) (c)

Figure 7. (a) Photo of the imaging setup with the G3 sensor, scanning mirror, and three different thin targets placed at similar height. The scanning area is marked by the white dashed region. The reconstructed 2D (b) US and (c) OA images of the three targets. The color bar represents the normalized signal amplitude.

C. 3D Imaging of Thin Targets at Different Heights

The same setup (Fig. 7(a)) is used to further demonstrate the 3D imaging capability of the G3 sensor, except using three 1-mm-ϕ black coaxial cables at different heights as targets (Fig. 8(a)). The horizontal and vertical spacing is 2 mm and 4 mm, respectively, making the air gap between two adjacent cables around 1 mm (horizontal) and 3 mm (vertical). The same voltage range and step size are used to drive the scanning mirror, providing the same scanning area, as marked by the white-dashed region, with around 13 mm range in height. The 3D US and OA images (Fig. 8(b) and 8(c)) are reconstructed by stacking the B-scan images acquired at the 11 tilt steps. The normalized signal amplitude at each location (pixel) is indicated by the color bar. Each B-scan image is reconstructed by the 31 A-scan signals during one scan in pan. In both US and OA images, the three coaxial cables are resolved clearly.

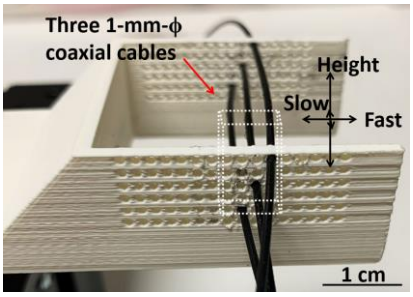

(a)

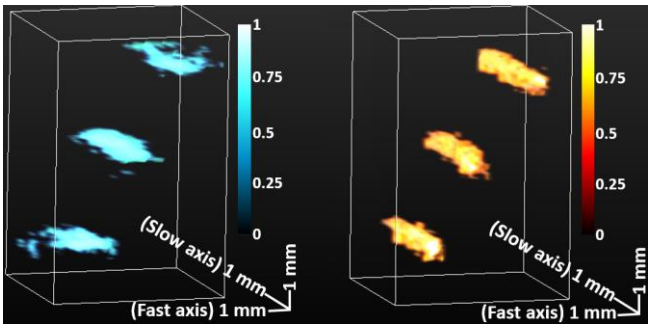

(b) (c)

Figure 8. (a) Photo of the 3D imaging targets at different heights. The reconstructed 3D (b) US and (c) OA images of the three black coaxial cables. The color bar represents the normalized signal amplitude.

V. Conclusion and Future Work

In this paper, we have demonstrated the G3 DMDSM sensor for near-distance pulse-echo ultrasound and OA ranging and imaging. Different from the previous versions, a new US/OA transceiver has been designed to generate self-focused laser and ultrasound beams without the need of a (bulky) parabolic reflector. This makes it possible to further miniaturize the DMDSM sensor to make it suitable for robotic finger-tip operations. In addition, the self-focused laser and ultrasound beams can be easily steered by a 2D scanning mirror for not only single-point ranging and detection but also areal mapping or imaging. Due to lower NA of focusing, the lateral resolution of the US/OA modalities somewhat deteriorates, which however should be good enough for most grasping applications. On the other hand, the effective work range has been significantly enlarged and two focal zones better overlap with each other. These features could better facilitate the grasping of targets with more complex shapes or surface features.

In the future, the miniaturization of both the DMDSM sensor and the scanning mirror as well as their seamless integration will be investigated. A new laser source with high PRR will be explored to boost the scanning speed and reduce the imaging time. These improvements are expected to make the DMDSM sensor more practical to be used on a robotic hand for grasping operations.

Acknowledgment

The authors would like to thank for the inputs and feedback from Xiaoyu Duan.

References

[1] M. T. Mason, Mechanics of Robotic Manipulation, MIT press, 2001.

[2] M. Ciocarlie, K. Hsiao, E.G. Jones, S. Chitta, R.B. Rusu and I.A. Şucan, "Towards reliable grasping and manipulation in household environments," *Experimental Robotics,* pp. 241-252, Springer, Berlin, Heidelberg, 2014.

[3] K. Y. Goldberg, "Orienting Polygonal Parts Without Sensors," *Algorithmica,* vol. 10, no. 2-4, pp. 201-225, 1993.

[4] M. A. Erdmann and M. T. Mason, "An exploration of sensorless manipulation," *IEEE Journal on Robotics and Automation,* vol. 4, no. 4, pp. 369-379, 1988.

[5] C. E. Smith and N. P. Papanikolopoulos, "Vision-Guided Robotic Grasping: Issues and Experiments," *Proceedings of IEEE International*

Conference on Robotics and Automation, vol. 4, pp. 3203-3208, 1996.

[6] A. Wehr and U. Lohr, "Airborne laser scanning—an introduction and overview," *ISPRS Journal of photogrammetry and remote sensing,* vol. 54, no. 2-3, pp. 68-82, 1999.

[7] Y. Lu, J. Lee, S. H. Yeh, H. M. Cheng, B. Chen and D. Song, "Sharing Heterogeneous Spatial Knowledge: Map Fusion between Asynchronous Monocular Vision and Lidar or Other Prior Inputs," *Robotics Research,* pp. 727-741, Springer, Cham, 2020.

[8] M. C. Amann, T. M. Bosch, M. Lescure, R. A. Myllylae and M. Rioux, "Laser ranging: a critical review of unusual techniques for distance measurement," *OptEn,* vol. 40, pp. 10-19, 2001.

[9] A. Stelzer, M. Jahn and S. Scheiblhofer, "Precise distance measurement with cooperative FMCW radar units," *2008 IEEE Radio and Wireless Symposium,* pp. 771-774, 2008.

[10] R. D. Howe, "Tactile sensing and control of robotic manipulation," *Advanced Robotics,* vol. 8, no. 3, pp. 245-261, 1993.

[11] J. M. Romano, K. Hsiao, G. Niemeyer, S. Chitta and K. J. Kuchenbecker, "Human-Inspired Robotic Grasp Control With Tactile Sensing," *IEEE Transactions on Robotics,* vol. 27, no. 6, pp. 1067-1079, 2011.

[12] Q. Xu, "Design and Development of a Novel Compliant Gripper With Integrated Position and Grasping/Interaction Force Sensing," *IEEE Transactions on Automation Science and Engineering,* vol. 14, no. 3, pp. 1415 - 1428, 2015.

[13] J. R. Smith, E. Garcia, R. Wistort and G. Krishnamoorthy, "Electric field imaging pretouch for robotic graspers," *2007 IEEE/RSJ International Conference on Intelligent Robots and Systems,* pp. 676-683, 2007.

[14] R. Wistort and J. R. Smith, "Electric field servoing for robotic manipulation," *In 2008 IEEE/RSJ International Conference on Intelligent Robots and Systems,* pp. 494-499, 2008, September.

[15] B. Mayton, L. LeGrand and J. R. Smith, "An electric field pretouch system for grasping and co-manipulation," *2010 IEEE International Conference on Robotics and Automation,* pp. 831-838, 2010.

[16] B. Mayton, E. Garcia, L. LeGrand and J. R. Smith, "Electric field pretouch: Towards mobile manipulation," *In RSS Workshop on Mobile Manipulation in Human Environments,* 2009, June.

[17] K. Hsiao, P. Nangeroni, M. Huber, A. Saxena and A. Y. Ng, "Reactive grasping using optical proximity sensors," *2009 IEEE International Conference on Robotics and Automation,* pp. 2098-2105, 2009.

[18] B. Yang, P. Lancaster and J. R. Smith, "Pre-touch sensing for sequential manipulation," *2017 IEEE International Conference on Robotics and Automation (ICRA),* pp. 5088-5095, 2017.

[19] H. Hasegawa, Y. Mizoguchi, K. Tadakuma, A. Ming, M. Ishikawa and M. Shimojo, "Development of intelligent robot hand using proximity, contact and slip sensing," *In 2010 IEEE International Conference on Robotics and Automation,* pp. 777-784, 2010, May.

[20] A. Maldonado, H. Alvarez and M. Beetz, "Improving robot manipulation through fingertip," *In 2012 IEEE/RSJ International Conference on Intelligent Robots and Systems,* pp. 2947-2954, 2012.

[21] L. Jiang and J. R. Smith, "A unified framework for grasping and shape acquisition via pretouch sensing," *In 2013 IEEE International Conference on Robotics and Automation,* pp. 999-1005, 2013, May.

[22] E. Guglielmelli, V. Genovese, P. Dario and G. Morana, "Avoiding obstacles by using a proximity us/ir sensitive skin," *In Proceedings of 1993 IEEE/RSJ International Conference on Intelligent Robots and Systems (IROS'93),* vol. 3, pp. 2207-2214, 1993, July.

[23] L. Jiang and J. R. Smith, "Seashell effect pretouch sensing for robotic grasping," *In 2012 IEEE International Conference on Robotics and Automation,* pp. 2851-2858, 2012, May.

[24] L. T. Jiang and J. R. Smith, "Pretouch sensing for manipulation," *In Robotics: Science and Systems (RSS) Workshop: Alternative Sensing Techniques for Robotic Perception,* 2012, July.

[25] C. Fang, D. Wang, D. Song and J. Zou, "The Second Generation (G2) Fingertip Sensor for Near-Distance Ranging and Material Sensing in Robotic Grasping," *IEEE 2022 International Conference on Robotics and Automation (ICRA),* pp. 1506-1512, 2022, May.

[26] D. Wang, F. Guo, C. Fang, J. Zou and D. Song, "Design of an Object Scanning System and a Calibration Method for a Fingertip-Mounted Dual-Modal and Dual Sensing Mechanisms (DMDSM)-based Pretouch Sensor for Grasping," *IEEE International Conference on Automation Science and Engineering (CASE),* 2022, August.

[27] C. Fang, D. Wang, D. Song and J. Zou, "Fingertip Pulse-Echo Ultrasound and Optoacoustic Dual-Modal and Dual Sensing Mechanisms Near-Distance Sensor for Ranging and Material Sensing in Robotic Grasping," *IEEE International Conference on Robotics and Automation (ICRA),* 2021.

[28] C. Fang, D. Wang, D. Song and J. Zou, "Toward Fingertip Non-Contact Material Recognition and Near-Distance Ranging for Robotic Grasping," *2019 IEEE International Conference on Robotics and Automation (ICRA),* pp. 4967-4974, 2019.

[29] C. Fang, D. Wang, D. Song and J. Zou, "Fingertip Non-Contact Optoacoustic Sensor for Near-Distance Ranging and Thickness Differentiation for Robotic Grasping," *2020 IEEE/RSJ International Conference on Intelligent Robots and Systems (IROS),* pp. 10894-10899, IEEE, 2020.

[30] X. Duan, D. Wang, D. Song and J. Zou, "Device Design and System Integration of a Two-Axis Water-immersible Micro Scanning Mirror (WIMSM) to Enable Dual-modal Optical and Acoustic Communication and Ranging for Underwater Vehicles," *IEEE International Conference on Robotics and Automation (ICRA),* pp. 13114-13119, 2021, May.